Journal of Applied Polymer Science

Light-scattering capacity of ethylene–vinyl acetate copolymers in polypropylene: Toward high haze and transmittance

Shanshan Luo, Ping Yi, Ying Xiong, Jiabin Shen, Shaoyun Guo

State Key Laboratory of Polymer Materials Engineering, Polymer Research Institute of Sichuan University, Chengdu 610065, China

Correspondence to: J. Shen (E-mail: shenjb@scu.edu.cn) and S. Guo (E-mail: nic7702@scu.edu.cn)

ABSTRACT: Light-scattering materials were fabricated by the melt blending of polypropylene with an ethylene–vinyl acetate copolymer (EVA) to prevent the glare effect of light-emitting diodes. The results show that the light-scattering capacity was remarkably dependent on the phase morphologies of EVA. (1) When EVA was dispersed as spherical droplets, the transmittance and haze gradually increased with the enrichment of EVA, and the half-peak width of the light-scattering pattern reached a maximum when 30 wt % EVA was loaded. On the basis of the analysis of Mie scattering theory, the enlargement of scattering particles promoted light transmittance, and more incoming light was deflected at the arclike interfaces. This induced a distinct antiglare effect. (2) When scattering particles deformed and expanded vertically in the light-transmitting direction, the light-scattering capacity turned out to be weakened by further enrichment of the EVA phase. The planelike interfaces reduced the deflection of incoming light, and this led to decreases in the scattering angles. © 2015 Wiley Periodicals, Inc. J. Appl. Polym. Sci. **2016**, *133*, 42844.

KEYWORDS: blends; light scattering; polyolefins

Received 25 May 2015; accepted 14 August 2015
DOI: 10.1002/app.42844

INTRODUCTION

With the remarkable growth of the light-emitting diode (LED) industry, greater challenges have been placed in the way of ideal applications.[1–6] To replace conventional lighting systems, alternatives with high performance and low cost must be developed to meet market requirements.[7–10] For example, to prevent the glare effect of LEDs, light-scattering plates play critical roles in providing the effective distribution of light sources.[11–15] Instead of the materials [e.g., polycarbonate,[11,12,16] poly(methyl methacrylate),[17–19] poly(ethylene terephthalate)[20]] applied as the matrixes of the present products, increasing attention has been focused on other low-cost candidates.

As one semicrystalline polymer, polypropylene (PP) is widely applied in various fields. Because of the distinction between the refractive indices of the crystalline and amorphous regions, neat PP commonly has a high haze value, but good transparency could also be achieved by the control of its crystallization or the size of the crystallites.[21–24] However, it is widely recognized that optical transmittance and haze are inversely proportional values in most cases.[4,16,21,22] For example, by the addition of only small amounts of nucleating agents (~1.0 wt %) to the neat PP, the transmittance increased beyond 95% from 80%; this was accompanied by a distinct decrease in the optical haze.[21] Thus, obtaining both high transmittance and haze values is a great challenge for PP, as a candidate as a light-scattering material for LED lighting systems.

Among the key parameters of light-scattering properties, haze is characterized by the percentage of light that is deflected more than 2.5° from the incoming light direction.[25] To obtain a high haze value, filling foreign inorganic particles (e.g., $BaSO_4$, $CaCO_3$, TiO_2 and ZnO) acting as the light-scattering phase is regarded as an effective method.[16,26] However, a distinct difference in the refractive index between the particles and polymeric matrix may not only provide the composite material with a high haze value but may also cause a negative effect on the optical transmittance. In addition, the particle distribution and migration, surface roughness, and processability may also become a hindrance for the application of this kind of material.[25] In recent years, the blending of the organic scattering phase [e.g., poly(methyl methacrylate), acrylic resin, poly(styrene-*co*-acrylonitrile), etc.] with a polymeric matrix has attracted extensive interest.[14,27,28] In comparison with inorganic fillers, the polymeric phase is more deformable in melt processing. On the basis of Mie scattering theory, the scattering efficiency (K) of a scattering particle is mainly dependent on its shape, dimension, refractive index, and so on. On the other side, to maintain a high light transmittance, the scattering phase with a close refractive index to that of the matrix would be the best choice.[6,10] This suggests that K of the organic dispersed phase could

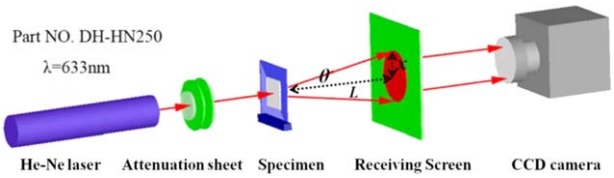

Figure 1. Schematic of the measuring system of light-scattering capacity. [Color figure can be viewed in the online issue, which is available at wileyonlinelibrary.com.]

be improved by the control of its morphologies, and this may provide a potential way to achieve an optimum light-scattering performance with high transmittance and haze values.

With regard to the low cost and ease of processability, two conventional thermoplastic polymers, PP and ethylene–vinyl acetate copolymer (EVA), were, chosen as the matrix and scattering phase, respectively, in a light-scattering material that was fabricated through melt-blending technology. As the scattering phase, EVA (with 18% vinyl acetate) with a refractive index of 1.4845 was dispersed in the PP matrix with a refractive index of 1.4735. Close refractive indices are considered to be capable of reducing the light reflection at interfaces. Different morphologies of EVA were obtained, and their influence on the light transmittance, haze, and light-scattering capacity of the whole blending material was investigated in this study. In addition, related mechanisms were proposed on the basis of Mie scattering theory.

Table I. Transmittance and Haze of the PP, EVA, and PP/EVA Blends

Sample name	Transmittance (%)	Haze (%)
Pure PP	81.6	83.1
Pure EVA	86.4	39
PV-1	81.2	90.8
PV-2	81.4	93.2
PV-3	82.3	93.6
PV-4	84.6	92.4
PV-5	84.8	90.6
PV-6	84.8	88.6

EXPERIMENTAL

Materials

Isotactic PP (M160E), with a melt index of 1.6 g/10 min, a density of 0.9 g/cm^3, and a refractive index of 1.4735, was produced by Sinopec Shanghai Petrochemical Co., Ltd. (China). EVA (18J3), with a melt index of 2.8 g/10 min, a density of 0.94 g/cm^3, and a refractive index of 1.4845, was obtained from Sinopec Beijing Yanshan Co. (China). The vinyl acetate content was 18%.

Specimen Preparation

The PP was first melt-blended with 10, 20, 30, 40, 50, and 60 wt % EVA (the blends are denoted as PV-1, PV-2, PV-3, PV-4, PV-5, and PV-6, respectively) in an internal mixer (Haake

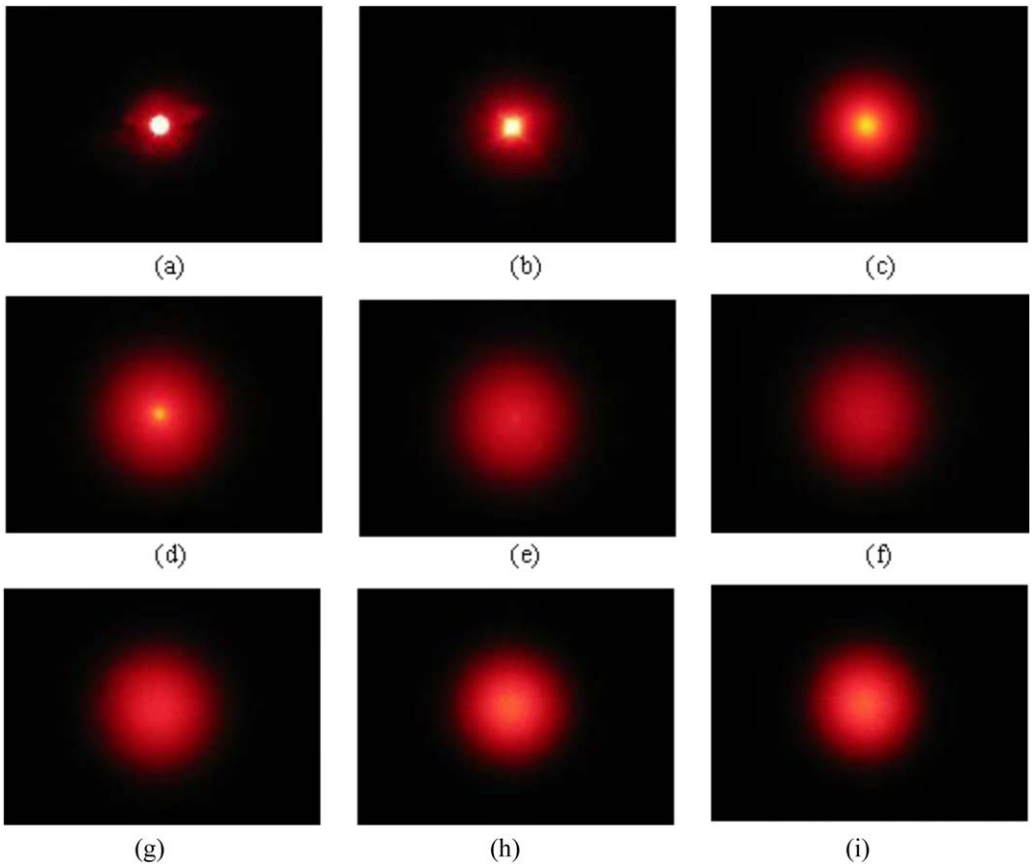

Figure 2. Light-scattering patterns of (a) a laser beam, (b) pure EVA, (c) pure PP, (d) PV-1, (e) PV-2, (f) PV-3, (g) PV-4, (h) PV-5, and (i) PV-6. [Color figure can be viewed in the online issue, which is available at wileyonlinelibrary.com.]

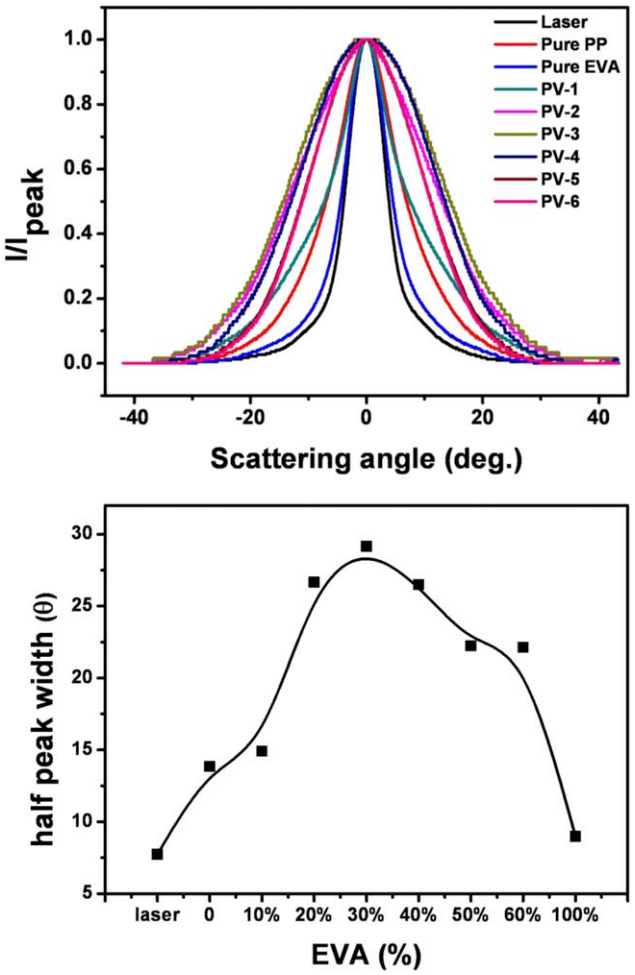

Figure 3. (a) Relative light intensity as a function of θ and (b) the half-peak width of the PP/EVA blends as a function of the weight percentage of EVA. [Color figure can be viewed in the online issue, which is available at wileyonlinelibrary.com.]

PolyLab QC) for 6 min at 200 °C and 30 rpm. Subsequently, the PP/EVA blending products were hot-pressed into circular-like samples at 200 °C for 7 min at 10 MPa and then cooled down at a rate of 25 °C/min with circulating water. The diameter and thickness of each sample were 25 mm and 1.7 mm, respectively.

Optical Properties

The transmittance and haze values of each sample were obtained through a transmittance/haze measuring machine (Shanghai Precision Instrument Co., China), which used a light source with a constant wavelength of 550 nm. At least of three specimens for each sample were tested, and the average value was calculated.

The light-scattering capacity of each sample was visually observed through a self-made instrument.[27,29] As schematically shown in Figure 1, the sample was mounted between a laser source and a receiving screen. When a laser beam with a wavelength of 633 nm passed through the sample, the pattern of transmitting light was projected on the screen and recorded by a camera. The distance between the sample and receiving screen is indicated by *L*, and the diameter of the light pattern projected on the screen is indicated by *x*; thus, the scattering angle (θ) of the transmitting light can be theoretically calculated with the follow equation:

$$\theta = \tan^{-1}(x/L)$$

Furthermore, the distribution of the relative light intensity could be obtained by the plotting of the relative light intensity of each recorded pattern at every pixel versus θ through Origin software.

We also evaluated the light-scattering capacity by mounting each sample on a set of LED units, and the photos were taken by a digital camera fixed above the specimen.

Micromorphological Observations

The polarized light microscopy (PLM) observation was performed with an Olympus BX51 polarizing microscope equipped with a heating cell. A thin slice about 10 μm in thickness was obtained by a microtome from each sample. To distinctly distinguish the phase regions between EVA and PP, each specimen was heated to 100 °C (beyond the melting temperature of EVA) for observation.

The fine morphology and particle size of dispersed EVA phase were observed and examined through scanning electron microscopy (SEM; JSM-5900LV, Japan). Each specimen was first cryo-fractured in liquid nitrogen, and the surface was coated with a layer of gold in a vacuum before observation. At least 10 images were collected to statistically analyze the size distribution and average diameter of dispersed EVA droplets.

RESULTS

Transmittance and Haze

The transmittance and haze values were measured through a transmittance/haze measuring machine with a light source with a constant wavelength of 550 nm. Three samples for each system were measured, and the results had good reproducibility (the difference was less than 0.2). Thus, the data reported in Table I were obtained from the average value of three samples. We found that the addition of 10 wt % EVA had little influence on the transmittance of the PP-based blend but induced a distinct increase of the haze from 83.1 to 90.8% compared to those of pure PP. Further enriching the concentration of the light-scattering phase to 60 wt %, the transmittance of the blends increased slightly to 84.8%, whereas the haze reached a maximum value of 93.6% when 30 wt % EVA was loaded. In a desired light-scattering material that can provide appropriate light distribution and prevent the glare effect of LED light, both a high transmittance and high haze are required. However, it is widely recognized that these two parameters are inversely proportional values in most cases.[4,16,21,22] For example, Zhou and Burkhart[25] reported that when 4 vol % SiO_2 was filled, the haze of polycarbonate was increased to about 88% from 25%, whereas the transmittance was reduced to 47 from 89%. Thus, the significance of the PP/EVA system reported in this study provided a kind of potential candidate for light-scattering material. The addition of EVA not only increased the haze but also maintained a stable transmittance. It should be noted that the thickness dependence on the optical properties of previous specimens was not considered in this study to prevent the influence of morphological development through a reduction in the thickness.

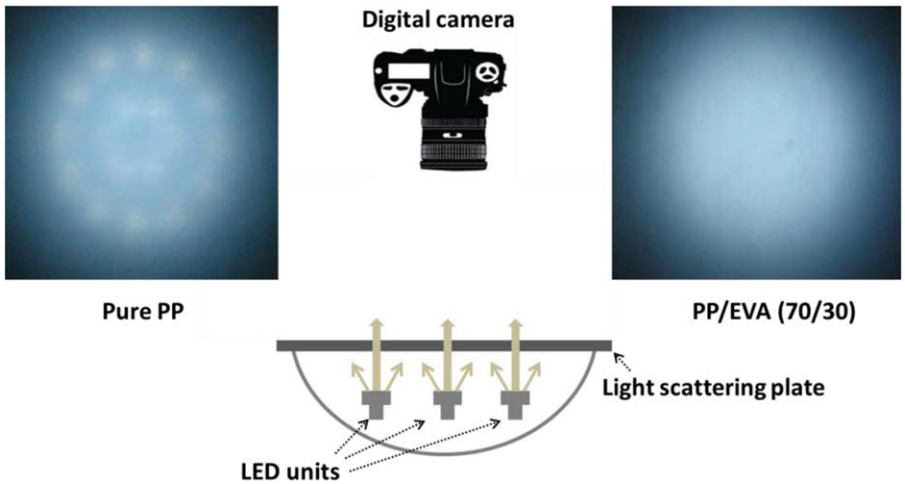

Figure 4. Schematic of the antiglare effect of a light-scattering plate and photo images of LED light transmission through (left) pure PP and (right) PV-3 plates. [Color figure can be viewed in the online issue, which is available at wileyonlinelibrary.com.]

Light-Scattering Capacity

The light-scattering capacity was visualized through the application of a laser passing through a specimen.[27,29] As displayed in Figure 2, when a laser was directly projected on a screen, a glare spot was recorded. For comparison, the scattering patterns of the pure PP and EVA were also recorded, respectively. We observed that although the glare effect at the spot center still existed, the scattering area of PP was distinctly larger than that of EVA; this indicated that the former one was able to lead more light being scattered because of the different refractive indices between the crystalline and amorphous regions. Moreover, when EVA was blended with PP, the glare at the spot center tended to disappear, and the scattering pattern became more homogeneous with increasing concentration of EVA, whereas the glare effect was strengthened when more than 30 wt % EVA was added.

For quantitative analysis, the relative light intensity at different θ was captured by the integration of each scattering pattern so that the scattering capacity could be evaluated through the half-peak width (i.e., θ as the relative light intensity reached 50%). The results included in Figure 3 exhibit that the curves became wider with the addition of EVA, and the half-peak width approached a maximum (∼29°) when the concentration of the dispersed phase reached 30 wt %. This tendency was basically consistent with the measured values of the haze (Table

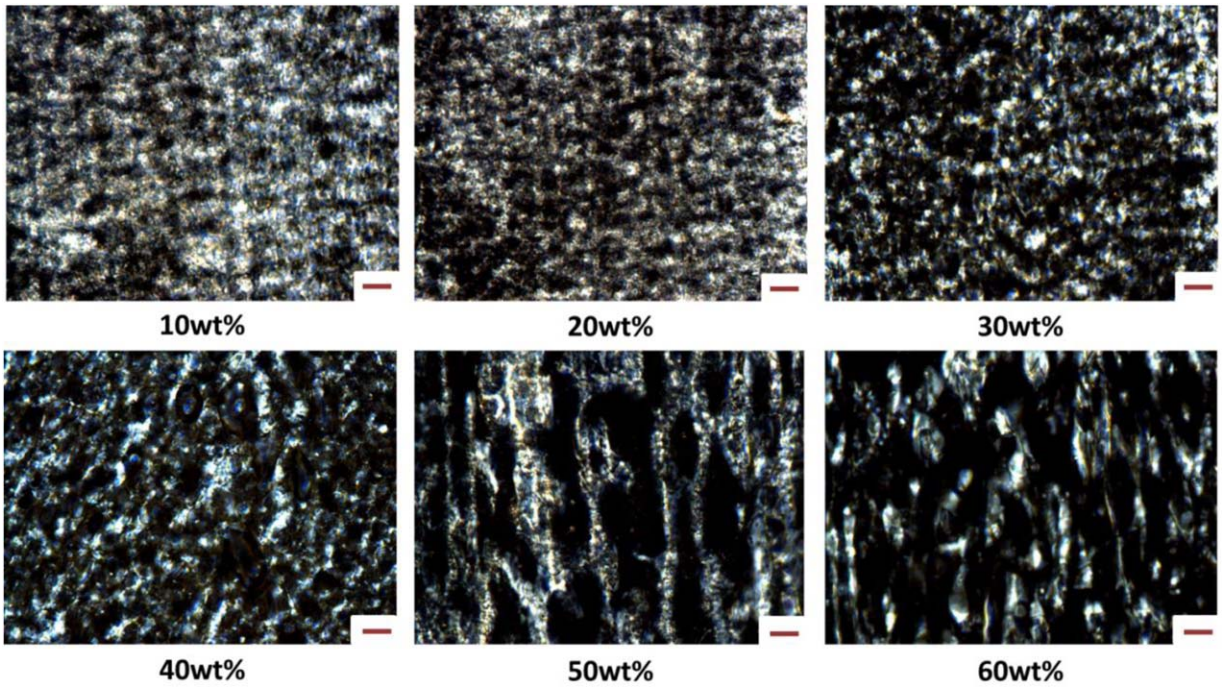

Figure 5. PLM images of the PP/EVA materials blended with different concentrations of the EVA phase (scale bar = 20 μm). [Color figure can be viewed in the online issue, which is available at wileyonlinelibrary.com.]

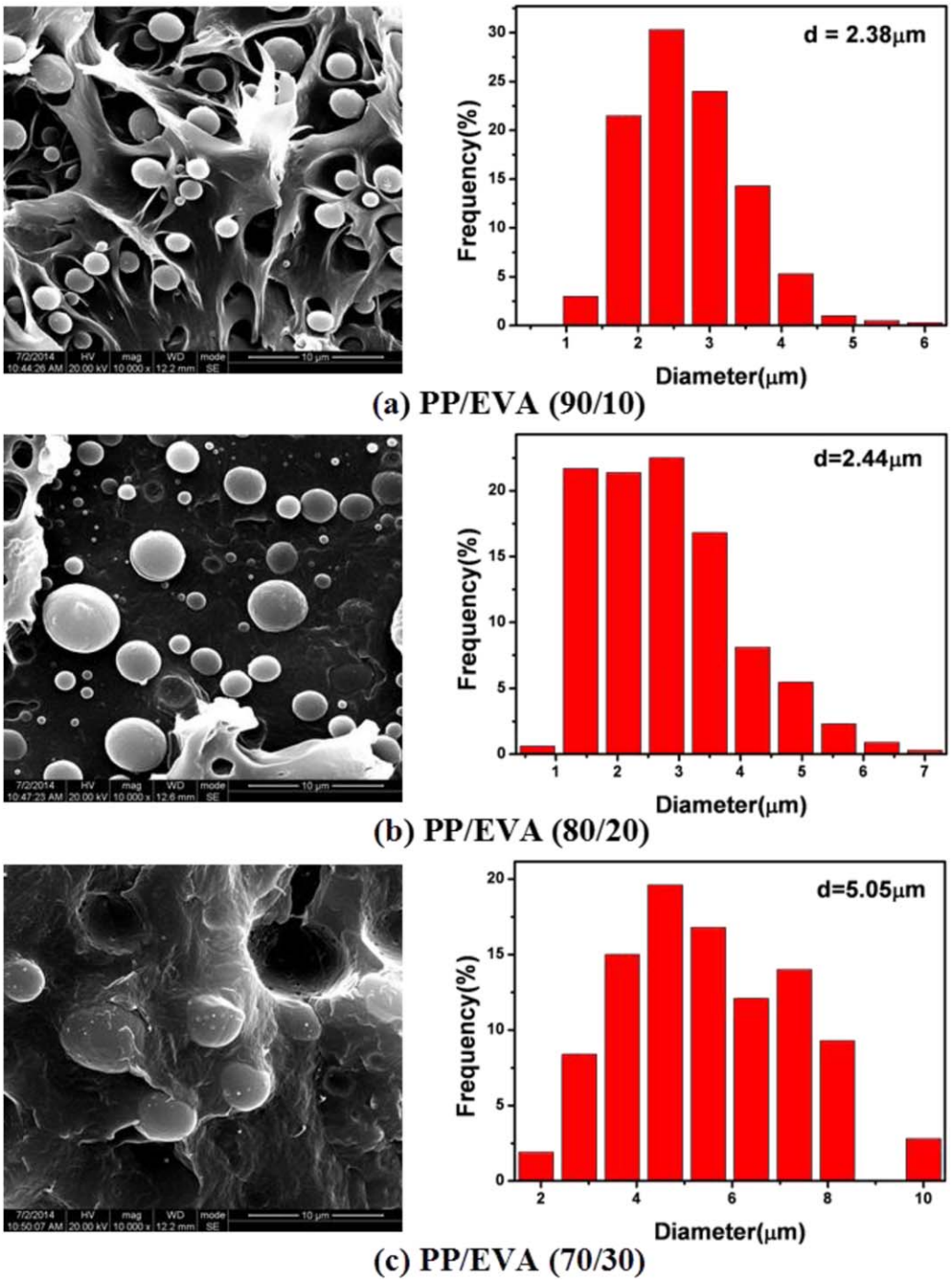

Figure 6. (left) SEM images and (right) size distribution of the PP/EVA materials blended with (a) 10, (b) 20, and (c) 30 wt % of the EVA phase. [Color figure can be viewed in the online issue, which is available at wileyonlinelibrary.com.]

I) and the observed scattering patterns (Figure 2); this suggests that an appropriate concentration of EVA would provide an optimal light distribution for the antiglare effect.

The light-scattering capacities of the pure PP and PV-3 were further compared by the mounting of each material on a set of LED units, and the photos were taken at the same distance as schematically shown in Figure 4. When the LED light was transmitted through the pure PP, each light unit was observed clearly; this indicated a higher haze would be required to prevent the glare effect. When 30 wt % EVA was blended with PP, the light units disappeared, and an improved light distribution was obtained; this induced a distinct antiglare effect.

DISCUSSION

Because the light-scattering capacity mainly depended on the deflection of the transmission light from its incident direction

Table II. K, S_{single} and S_{total} Values

Sample name	Particle size (μm)	K	S_{single}	N	S_{total}
PP/EVA-10%	2.38	0.02	0.09	0.03	2.7×10^{-3}
PP/EVA-20%	2.44	0.02	0.10	0.06	6×10^{-3}
PP/EVA-30%	5.05	0.09	1.84	0.02	3.7×10^{-2}

occurring at the interfaces between the PP and EVA phases, the morphological evolution of the dispersed phase was observed through PLM. To distinctly distinguish the phase regions, each specimen was first heated to 100 °C, beyond the melting temperature of EVA. Thus, when observed under polarized light, the dark spots could be regarded as phase regions of EVA. In addition, it needs to be noted that the horizontal direction in each PLM image corresponded to the transmission direction of the light in optical measurements. The morphological evolution of the EVA phase observed in Figure 5 displays that as a minor phase, EVA was separately dispersed in the PP matrix as spherical particulates. The particulate numbers and dimensions enlarged with increasing concentration of the dispersed phase. When more than 40 wt % EVA was added, the dispersed phase became continuous with a high aspect ratio and tended to be oriented vertically to the thickness direction of the whole specimen because of the confinement effect of the hot-press processing. For the morphological difference, the different tendencies of the optical properties to the concentration of EVA were further examined.

0–30 wt % EVA

The morphologies and dimensions of the dispersed EVA phase were carefully examined through SEM observation at a larger magnification (10,000×). As shown in Figure 6, it was distinctly demonstrated that the spherelike EVA droplets were separately dispersed in the PP matrix, and their average diameters increased from 2.38 to 5.05 μm when the concentration of EVA increased from 10 to 30 wt %. It needs to be noted that enriching the concentration of EVA may have induced the increase in the particle size or numbers. Thus, the small change in the average diameters with the enrichment of EVA from 10 to 20% could be ascribed to the increase in the particle numbers.

It is known that the size of light-scattering agents is regarded as one of crucial factors in determining the light-scattering capacity in a material based on Mie scattering theory. According to the equations in Appendix, the K and total scattering area (S_{total}) values of the PP/EVA blends with different sizes of the EVA phase were calculated and are summarized in Table II. The results reveal that both K and S_{total} increased synchronously with the enlargement of scattering particles, and this quantitatively indicated that the larger particle provided a higher K. Furthermore, the calculated single scattering profiles of each specimen were also obtained according to the equations in Appendix and compared in Figure 7. Two kinds of scattering methods are included, namely, forward directional (black lines) scattering and backward directional (red lines) scattering. The former corresponds to the light transmittance capacity through a scattering particle, whereas the latter characterizes the light reflection from the same particle. The results show that as the average diameter increased to 5.05 μm, the backward directional scattering weakened (which was observed by a magnification of six orders of magnitude), whereas the forward directional scattering tended to be strengthened. This revealed that the larger size of the scattering phase induced a higher light transmittance that was accompanied by a decrease in the reflection effect. Thus, we considered that the higher haze and transmittance obtained by the blending of more EVA phase in the PP matrix (see Table I) was due to the enlargement of the scattering phase on the basis of previous calculated results. However, this tendency was contrary to that reported for other materials. Increasing the concentration of undeformable light-scattering agents commonly causes a negative influence on the light transmittance, although the haze may be improved distinctly.

40–60 wt % EVA

When more than 40 wt % EVA was blended, the increased dimensions and aspect ratio of the dispersed phase led the Mie

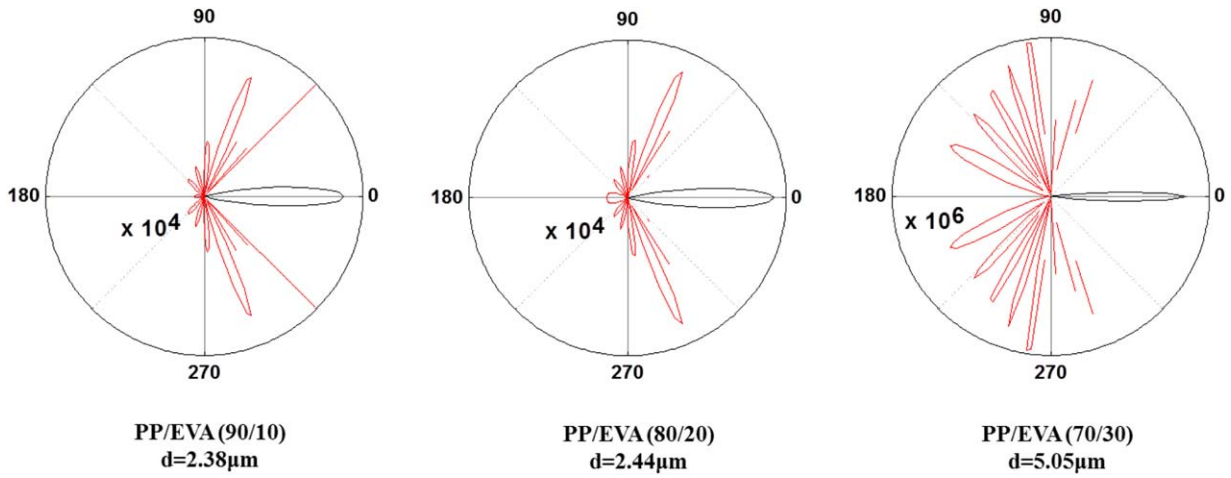

Figure 7. Calculated single scattering profiles of the PP/EVA blends with different particle sizes based on Mie scattering theory. The red lines are the magnified diagrams, and the magnification is marked next to them. [Color figure can be viewed in the online issue, which is available at wileyonlinelibrary.com.]

scattering theory to be declared invalid. It is known that when passing through a dual-phase material, incident light will be reflected or deflected at interfaces because of the different refraction indices between adjacent phases. Thus, the number and location of the interfaces will play significant roles in influencing the light transmittance and scattering capacity. According to the PLM images shown in Figure 5, the enriched EVA phase became continuous because of the coalescence effect; we considered this to induce more incident light-transmitting through the continuous channels so that the measured light transmittance of the whole material was beyond 84.5% and got closer to that of pure EVA (see Table I). Moreover, with the enlargement of the phase dimensions, the EVA phase tended to be compressed because the confinement effect of the hot-press processing led more interfaces to be oriented vertically to the thickness direction of the whole specimen. Thus, when the light was incident parallel to the thickness direction of the material, the θ at the interfaces became weakened; this resulted in decreases in the haze and scattering capacity of the material.

CONCLUSIONS

PP/EVA light-scattering materials were fabricated through melt-blending technology. With increasing concentration of EVA, its morphology evolved from spherical to expanded particles, which played a significant role in the light-scattering efficiency of the whole material. (1) When EVA was dispersed in the PP matrix as spherical droplets (0–30 wt % EVA), the transmittance and haze were gradually increased through the enrichment of the EVA phase, and the half-peak width of the light-scattering pattern reached a maximum (~29°) as 30 wt % EVA was added. This indicated that the scattering droplets provided effective light distribution for the antiglare effect. The analysis of Mie scattering theory further revealed that with the enrichment of the concentration of EVA, the average diameter of the dispersed particles increased from 2.38 to 5.05 μm; this promoted more incoming light to be deflected at the arclike interfaces and induced a distinct antiglare effect. (2) When the deformable EVA phase was expanded vertically to the light-transmitting direction (40–60 wt % EVA), the light-scattering capacity was weakened, and the haze decreased to 88.6% as 60 wt % EVA was added. The planelike interfaces were considered to reduce the deflection of incoming light and to lead to a decrease in θ.

ACKNOWLEDGMENTS

The authors are grateful to the National Natural Science Foundation of China (contract grant numbers 51203097, 51227802, 51420105004, and 51421061) for financial support of this study.

APPENDIX

On the basis of Mie scattering theory, the light-scattering intensity (I) and the scattering efficiency (K) of a single particle could be calculated through following equations:

$$\mathrm{I}(\alpha, m, \theta) = \lambda^2(i_1+i_2)/8\pi^2 \tag{A.1}$$

$$K(\alpha, m) = \left(\frac{\lambda^2}{2\pi^2 r^2}\right)\sum_{n=1}^{\alpha}(2n+1)\{|a_n|^2+|b_n|^2\} \tag{A.2}$$

$$i_1 = \left|\sum_{n=1}^{\infty}\frac{2n+1}{n(n+1)}\left\{a_n\frac{P_n^1(\cos\theta)}{\sin\theta}+b_n\frac{dP_n^1(\cos\theta)}{d\theta}\right\}\right|^2 \tag{A.3}$$

$$i_2 = \left|\sum_{n=1}^{\infty}\frac{2n+1}{n(n+1)}\left\{b_n\frac{P_n^1(\cos\theta)}{\sin\theta}+a_n\frac{dP_n^1(\cos\theta)}{d\theta}\right\}\right|^2 \tag{A.4}$$

$$a_n = \frac{\varphi_n(\alpha)\varphi_n'(m\alpha)-m\varphi_n'(\alpha)\varphi_n(m\alpha)}{\zeta_n(\alpha)\varphi_n'(m\alpha)-m\zeta_n'(\alpha)\varphi_n(m\alpha)} \tag{A.5}$$

$$b_n = \frac{m\varphi_n'(\alpha)\varphi_n(m\alpha)-\varphi_n(\alpha)\varphi_n'(m\alpha)}{m\zeta_n'(\alpha)\varphi_n(m\alpha)-\zeta_n(\alpha)\varphi_n'(m\alpha)} \tag{A.6}$$

$$\alpha = \frac{2\pi r n_m}{\lambda} \tag{A.7}$$

$$m = \frac{n_p}{n_m} \tag{A.8}$$

where i_1 and i_2 are the light-scattering intensity functions, a_n and b_n are the Mie scattering coefficients, α is the size parameter, m is the ratio of the refractive index of the particle (n_p) and the matrix (n_m), r is the particle radius, and λ is the wavelength of the incident light in the matrix. P_n^1 (cos θ) represents a Legendre polynomial, and φ_n and ζ_n are the first two orders of Ricatti–Bessel functions.

In addition, the scattering area of a single particle (S_{single}), which is quantitatively representative of the scattering capacity of the particle, could be calculated through eq. (A.9):

$$S_{\mathrm{single}} = K\frac{\pi d^2}{4} \tag{A.9}$$

where d is the average diameter of a particle. Thus, the S_{total} values of the particles dispersed in each specimen could be obtained as follows:

$$S_{\mathrm{total}} = NK\frac{\pi d^2}{4} \tag{A.10}$$

$$N = \frac{6\Phi}{\pi d^3} \tag{A.11}$$

where N is the number of particles in a specimen and Φ is the volume fraction of the particles.

REFERENCES

1. Song, S.; Sun, Y.; Lin, Y.; You, B. *Appl. Surf. Sci.* **2013**, *273*, 652.
2. Kim, G. H.; Kim, W. J.; Kim, S. M.; Son, J. G. *Displays* **2005**, *26*, 37.
3. Ignell, S.; Rigdahl, M. *J. Appl. Polym. Sci.* **2012**, *124*, 1624.
4. Kuo, H. P.; Chuang, M. Y.; Lin, C. C. *Powder Technol.* **2009**, *192*, 116.
5. Ishinabe, T.; Nakayama, T.; Miyashita, T.; Uchida, T. *Jpn. J. Appl. Phys.* **2004**, *43*, 6152.
6. Sun, Z.; Chang, J.; Zhao, N.; Jin, W.; Wang, Y. *Opt.—Int. J. Light Electron Opt.* **2010**, *121*, 760.
7. Johnson, P. M.; Gómez Rivas, J.; Bret, B. P. J.; Lagendijk, A.; Kelly, J. *J. Phys. Rev. Lett.* **2002**, *89*, 243901.
8. Veniaminov, A.; Bartsch, E. *J. Opt. A: Pure Appl. Opt.* **2002**, *4*, 387.
9. Hsu, C.; Lin, H.; Wu, W. *Thin Solid Films* **2009**, *517*, 3717.

10. Tagaya, A.; Ishii, S.; Yokoyama, K.; Higuchi, E.; Koike, Y. *Jpn. J. Appl. Phys.* **2002**, *41*, 2241.
11. Seo, J.; Cha, S. W.; Kim, H. B., *Polym.–Plast. Technol.* **2009**, *48*, 351.
12. Marek, M.; Steidl, J. *J. Mater. Sci.* **2006**, *41*, 3117.
13. Ismail, W. A.; Ali, Z. A.; Puteh, R. *Adv. Mater. Sci. Eng.* **2012**, *2012*, 1.
14. Smith, G. B.; Jonsson, J. C.; Franklin, J. *Appl. Opt.* **2003**, *42*, 3981.
15. Nishizawa, M.; Sekiya, K.; Kawakami, T.; Uchida, T. B. *Chem. Soc. Jpn.* **2012**, *85*, 839.
16. Zhao, Y.; Ding, P.; Ba, C.; Tang, A.; Song, N.; Liu, Y.; Shi, L. *Displays* **2014**, *35*, 220.
17. Kim, G. *Eur. Polym. J.* **2005**, *41*, 1729.
18. Guo, S.; Zhou, S.; Li, H.; You, B. *J. Colloid Interface Sci.* **2015**, *448*, 123.
19. Colombo, A.; Tassone, F.; Santolini, F.; Contiello, N.; Gambirasio, A.; Simonutti, R. *J. Mater. Chem. C* **2013**, *1*, 2927.
20. Shin, K.; Kim, H.; Cho, J.; Moon, S. J.; Kim, J. W.; Suh, K. *Macromol. Res.* **2012**, *20*, 385.
21. Kristiansen, M.; Werner, M.; Tervoort, T.; Smith, P.; Blomenhofer, M.; Schmidt, H. *Macromolecules* **2003**, *36*, 5150.
22. Kristiansen, P. M.; Gress, A.; Smith, P.; Hanft, D.; Schmidt, H., *Polymer* **2006**, *47*, 249.
23. Tenma, M.; Mieda, N.; Takamatsu, S.; Yamaguchi, M. *J. Polym. Sci. Part B: Polym. Phys.* **2008**, *46*, 41.
24. Mileva, D.; Androsch, R.; Radusch, H. *Polym. Bull.* **2009**, *62*, 561.
25. Zhou, R.; Burkhart, T. *J. Appl. Polym. Sci.* **2010**, *115*, 1866.
26. Mcneil, L. E.; French, R. H. *Acta Mater.* **2000**, *48*, 4571.
27. Huang, T.; Ciou, J.; Huang, P.; Hsieh, K.; Yang, S. *Opt. Express* **2008**, *16*, 440.
28. Wang, J.; Lien, S.; Ho, J.; Shih, T.; Chen, C.; Chen, C.; Whang, W. *Opt. Mater.* **2009**, *32*, 374.
29. Fang, Z.; Zhu, H.; Yuan, Y.; Ha, D.; Zhu, S.; Preston, C.; Chen, Q.; Li, Y.; Han, X.; Lee, S.; Chen, G.; Li, T.; Munday, J.; Huang, J.; Hu, L. *Nano Lett.* **2014**, *14*, 765.